Modeling and Optimization of the Carbon Dioxide to Methanol Process

Anna Midgley, Kane Norman, Nora Hallqvist

AM205: Advanced Scientific Computing
Harvard School of Engineering and Applied Sciences

December 2022

Abstract

This projects aims to accurately model the process of conversion of carbon dioxide to methanol in order to maximize the methanol production. To accomplish this, a range of numerical methods were used to solve various stages in the modeling process. Examples of such stages included solving differential equations in the reactor, root finding in the separator and optimization of the objective function given certain constraints. Specifically, four ODE solvers in the Runga-Kutta family and three root finding algorithms were analysed, in which Runga-Kutta method of order 4 (RK4) and Newton's method allowed for the greatest step size and least number of iterations respectively. The reactor and separator was solved for using RK4 and Newton's method, and validated by comparison to industry data. Lastly, projected gradient descent allowed for maximization of the methanol production whilst accounting for the physical and safety limitation of the system. We were able to improve the methanol production with 14.2%. Future work could investigate the effect of using an adaptive step size in projected gradient descent to find a better optimal, using an objective function based on cost and including more parameters as decision variables in optimization.

1 Introduction

Carbon dioxide (CO_2) is a greenhouse gas that is a major contributor to climate change. In order to combat this issue, there is a need to find ways to convert CO_2 into useful products. One potential solution is the conversion of CO_2 into methanol, which can be used as a fuel or chemical feedstock [6]. In this report, we analyze the numerical methods used in the modeling of the conversion of carbon dioxide to methanol, with the goal of selecting the most stable and convergent method. After which, we evaluate optimization of the process.

In this report, we will focus on analyzing several numerical methods for solving ordinary differential equations, including the forward Euler and higher order Runga-Kutta methods, as well as root finding methods such as bisection, Newton's, and chord. We will also consider the projected gradient descent method for constraint optimization. Our evaluation will prioritize convergence, stability, and accuracy in order to determine the most effective methods for the conversion of CO_2 to methanol.

Anna previously completed a chemical engineering undergraduate thesis in which she modeled the CO_2 to methanol process using Python and performed optimization on the system. While her original project relied on library packages for numerical methods, this project takes a different approach by implementing all numerical methods from scratch and comparing the convergence, stability, and accuracy of each. Our goal is to thoroughly analyze the stability and performance of these methods in order to select the most effective one for the CO_2 to methanol conversion process. Additionally, in this project we will consider different decision variables which will lead to an alternative formulation of the optimization problem. She used interior-point optimization that utilized both equality and inequality constraints. In this project, we will construct the problem such that only inequality constraints exist.

2 Modelling

2.1 Overview

A simplified flowsheet of the process can be seen in Figure 1. The production of methanol in a catalytic reactor (R-101) includes the hydrogenation of CO and CO_2 (reaction 1-2), as well as the reverse water-gas shift reaction (RWGS) (reaction 3). The output of the reactor is cooled to a temperature that allows for liquid methanol, the product, to be separated in a succeeding high-pressure flash separator (T-101). In order to simplify the modeling of the process, it was assumed that the process heat exchangers operated at their desired pressure and temperature values, thus leading to the required change in operating condition, but not requiring modeling of the energy transfer. Thus only the reactor and separator require detailed modeling of their mass and energy balances. The mass and energy balance across a unit are used to calculate the outlet streams given an inlet stream and operating conditions. It was assumed that the process operated at steady state. The following section describes the assumptions and design decisions that were made, and the resulting mathematical model of the system.

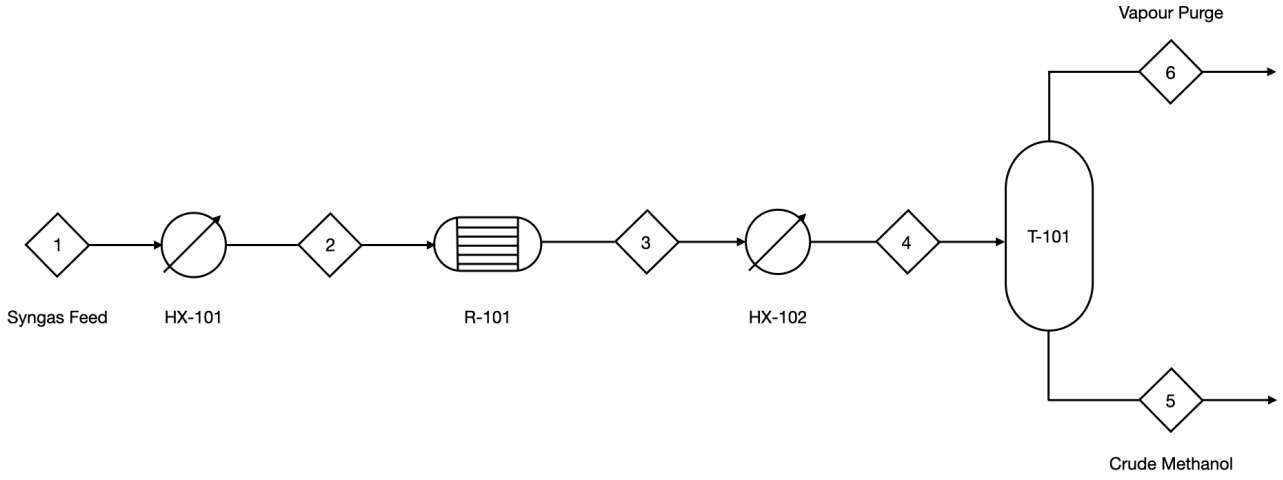

Figure 1: Simplified flowsheet of $C0_2$ to methanol process

$$CO + H_2 \leftrightarrow CH_3OH \tag{1}$$
$$CO_2 + 3H_2 \leftrightarrow CH_3OH + H_2O \tag{2}$$
$$CO_2 + H_2 \leftrightarrow CO + H_2O \tag{3}$$

2.1.1 Reactor Model

The methanol reactor model (R-101 from Figure 1) was based on a commercial tubular reactor with a packed bed of catalyst and counter-current coolant jacket. The fluid in the jacket was steam, which removes the exothermic heat of reactions. The mass and energy balances across the unit are described as a set of differential equations for the rate of change of composition and temperature along the reactor length. Due to the reactions that occur, the composition and temperature of the stream changes as it flows through the catalyst. The equations were derived from first principles and are given as,

$$\frac{dF_i}{dz} = N_t A_{\text{int}}\ \rho_{cat}\,(1-\varepsilon_{cat}) \sum_{i=1}^{N} r_i v_i \tag{4}$$

$$\frac{\partial T}{\partial z} = \left(\rho_{\text{cat}}\ a \sum_{i=1}^{n} r_i\,(-\Delta H_{f,i}) + \frac{4}{D_{\text{int}}} U\,(T_{\text{shell}}\ - T)\right)\left(\frac{N_t A_{int}\,(1-\varepsilon_{cat})}{f_{\text{t}} C_p}\right) \tag{5}$$

where f_{t} is total molar flowrate per tube, C_p is specific heat, ν_i is stoichiometric coefficient, r_i is the rate of reaction, z is the position in the reactor, F_i is component i's flowrate, and T is the temperature of the reactor [7]. The constants in the above equation were taken from literature and are given in Table 1 [1, 4].

An essential part of the reactor differential equations is the choice in kinetic model. The kinetic models are used to predict how a chemical reaction will progress and to understand the factors that affect the rate of the reaction. The kinetic model of the system described by Bussche and Froment, was used in the reactor modeling as recommended by multiple sources [2]. The kinetics of the reactor were described by the following rate expressions for the two rate-determining steps, the slowest steps that thus limits the overall rate of reaction,

Parameter	Symbol	Value	Units
Cross sectional area of reactor tube	A_{int}	0.00113	m^2
Void fraction of catalyst	ϵ_{cat}	0.39	
Density of catalyst	ρ_{cat}	1 100	kg/m^3
Activity of catalyst	a	1	
Internal diameter of reactor tube	D_{int}	0.038	m
Overall heat transfer coefficient	U	631	W/m^2K
Temperature of boiling water shell side	T_{shell}	511	K
Reactor length	z	7	m
Number of tubes	N_t	6560	
Number of species	N	7	
Number of reactions	n	3	

Table 1: Value of constants used in reactor mass and energy balance

$$r_{MeOH} = \frac{k_{\mathrm{MeOH}} p_{\mathrm{CO_2}} p_{\mathrm{H_2}} \left[1 - \left(\frac{1}{K^1_{eq}}\right)\left(p_{\mathrm{H_2O}} p_{\mathrm{CH_3OH}} / p^3_{\mathrm{H_2}} p_{\mathrm{CO_2}}\right)\right]}{\left(1 + K_1\left(p_{\mathrm{H_2O}}/p_{\mathrm{H_2}}\right) + K_{2\sqrt{2}} p_{\mathrm{H_2}} + K_3 p_{\mathrm{H_2O}}\right)^3} \tag{6}$$

$$r_{RWGS} = \frac{k_{RWGS} p_{CO_2} \left[1 - \left(\frac{1}{K^2_{eq}}\right)\left(p_{H_2O} p_{CO} / p_{CO_2} p_{H_2}\right)\right]}{\left(1 + K_1\left(p_{H_2O}/p_{H_2}\right) + K_{2\sqrt{2}}\sqrt{p_{H_2}} + K_3 p_{H_2O}\right)} \tag{7}$$

where p_i is the partial pressure of component i. The rate and equilibrium constants were determined from the following equations and associated constants [2, 4, 3, 10],

$$k = A \exp\left(\frac{B}{RT}\right) \tag{8}$$

$$K_{eq} = 10^{(A/T - B)} \tag{9}$$

	A	B
k_{MeOH}	1.07	36696
k_{RWGS}	$1.22 \cdot 10^{10}$	-94765
K_1	3453.38	-
K_2	0.499	17197
K_3	$6.62 \cdot 10^{-11}$	124119
K^1_{eq}	3066	10.592
K^2_{eq}	-2073	-2.029

Table 2: Value of constants in rate and equilibrium

Assumptions that were made for the reactor model include uni-dimensional flow, negligible axial diffusion, negligible heat conduction, no intra-particle diffusion limitations, no pressure drop across the reactor, and no accumulation of coolant in the jacket [3, 11]. These assumptions were used in various modeling and optimization studies of the process thus validating our decision to make them.

2.1.2 Separator Model

The high-pressure separator (T-101 from Figure 1) increases the pressure of the system, such that at equilibrium, the liquid phase is predominately methanol. The liquid (stream 5) can then be separated from the vapor (stream 6), thus separating a methanol rich stream from the rest of the chemical species. The effluent is predominately methanol and water with a low level of dissolved gases. The modeling of the separator requires determining the composition of its outlet streams and their flow rates. The mass balance over the unit for component i is given

by,

$$Fz_i = F_L x_i + F_V y_i \tag{10}$$

where z_i is mole fraction of component i in the separator feed, and y_i and x_i are respectively the product vapor and liquid mole fractions. To solve this system we used the given operating temperature, pressure and known inlet stream composition, to determine the unknown y_i, x_i, F_L and F_V. The Rachford-Rice equation given by,

$$\sum_{i=1}^{N} \frac{z_i \left(K_i - 1\right)}{1 + \left(\frac{F_V}{F}\right)\left(K_i - 1\right)} = 0 \tag{11}$$

can be used to determine the vapor flow rate F_V. Which can then be used together with the equilibrium ratio K_i to solve for the composition of component i in both the vapor and liquid outlet. Thus solving the overall mass balance over the separator. The process of determining K_i and F_V/F is iterative as both values depend on one another. The pseudo-code of how the system was solved is given by algorithm 1.

Algorithm 1 Solving K_i and F_V/F iteratively

1: Guess initial values for K_i and F_V/F
2: Calculate y_i and x_i by $x_i = \frac{F z_i}{F_L + F_V K_i}$ and $y_i = K_i x_i$
3: **for** $i \leftarrow 1$ to max iterations **do**
4: Use y_i and x_i to determine $K_{i,next}$
5: Using a root-finding method, calculate next iteration of the Rachford-Rice Equation 11 to determine new $F_{V,next}/F$
6: **if** $(F_{V,next} - F_V) <$ tolerance **then**
7: Break
8: **else**
9: $K_i \leftarrow K_{i,next}$ and $F_V \leftarrow F_{V,next}$

At the high pressure and temperature conditions, the compounds behavior deviates from ideality which cannot be disregarded in the separator modeling [4]. In order to account for the non-ideality, Equations of State are required to accurately determine the non-ideal vapor-liquid equilibrium (VLE) in the unit.

For this system, it is recommended that Peng Robinson Equations of State (PR-EOS) are used to determine the fugacity coefficients which are then used to calculate the equilibrium ratios (K_i) [4]. The polynomial form of PR-EOS are given by,

$$A = \frac{\alpha a p}{R^2 T^2} \tag{12}$$

$$B = \frac{bp}{RT} \tag{13}$$

$$Z^3 - (1 - B)Z^2 + \left(A - 2B - 3B^2\right) Z - \left(AB - B^2 - B^3\right) = 0 \tag{14}$$

where Z is the compressibility factor. The roots of the cubic equations are solved to determine Z for both the liquid and vapor phase of the mixture. This was done using `numpy.roots`. In order to determine a and b for the mixtures, empirical mixing rules are used to relate pure-component parameters to mixture parameters. The following mixture rules applies to the vapor phase,

$$a = \sum_{i=1}^{N} \sum_{j=1}^{N} y_i y_j a_{ij} \tag{15}$$

$$b = \sum_{i=1}^{N} y_i b_i \tag{16}$$

and the following for the liquid phase,

$$a = \sum_{i=1}^{N} \sum_{j=1}^{N} x_i x_j a_{ij} \tag{17}$$

$$b = \sum_{i=1}^{N} x_i b_i \tag{18}$$

with $a_{ij} = (1 - \delta_{ij})\, a_i^{1/2} a_j^{1/2}$. The binary interaction parameter for each component were obtained from experimental data and are shown in Table 3 [12].

	CO	CO_2	CH_3OH	H_2	H_2O	CH_4	N_2
CO	-	0	0	0.0919	0	0.03	0.033
CO_2	0	-	0.022	-0.1622	0.0063	0.0793	-0.0222
CH_3OH	0	0.022	-	0	-0.0778	0	-0.2141
H_2	0.0919	-0.1622	0	-	0	0.0263	0.0711
H_2O	0	0.0063	-0.0778	0	-	0	0
CH_4	0.03	0.0793	0	0.0263	0	-	0.0289
N_2	0.033	-0.0222	-0.2141	0.0711	0	0.0289	-

Table 3: Binary interaction parameters

The rest of terms in polynomial form of EOS are given by,

$$a_i = \left(0.457235 \frac{R^2 T_{c,i}^2}{P_{c,i}}\right) \alpha_i(T) \tag{19}$$

$$\alpha_i(T) = \left[1 + \kappa_i \left(1 - \sqrt{\frac{T}{T_{c,i}}}\right)\right]^2 \tag{20}$$

$$\kappa_i = 0.37464 + 1.5422 \cdot \omega_i - 0.26992 \cdot \omega_i^2 \tag{21}$$

$$b_i = 0.077796 \frac{RT}{P_{c,i}} \tag{22}$$

where $T_{c,i}$ and $P_{c,i}$ are the components critical temperature and pressure, and ω_i is its acentric factor. These values were obtained from literature and are given in Table 4.

	$T_{c,i}(K)$	$P_{c,i}(bar)$	ω_i
CO	132.9	35	0.066
CO_2	304.1	73.8	0.239
CH_3OH	512.6	80.9	0.556
H_2	33.0	12.9	-0.216
H_2O	647.3	221.2	0.344
CH_4	190.4	46	0.011
N_2	126.2	33.9	0.039

Table 4: Critical temperature, critical pressure and acentric factors of each components

Using the phase specific compressibility factor, the fugacity coefficient of the phase can be determined by,

$$\ln \phi_i = \frac{b_i}{b}(Z - 1) - \ln(Z - B) - \frac{A}{2\sqrt{2}B}\left(\frac{2}{a}\sum_i x_i (a)_{ij} - \frac{b_i}{b}\right) \ln \frac{Z + (1 + \sqrt{2})B}{Z + (1 - \sqrt{2})B} \tag{23}$$

Using the fugacity coefficient of both the vapor and liquid phase, the equilibrium ratio (K_i) for each component can be found by taking their ratio $K_i = \frac{y_i}{x_i} = \frac{\phi_i^L}{\phi_i^V}$.

3 Methods Overview

Our objective is to accurately model the conversion of carbon dioxide to methanol in order to maximize the methanol production. To accomplish this, we used numerical methods to solve a series of non-trivial tasks, specifically ordinary differential equations, finding roots of nonlinear functions, and optimization with constraints. We carefully selected the most appropriate numerical method for each problem in order to achieve accurate and efficient solutions.

We will evaluate and select from the following set of numerical methods to solve each task at hand:

- Ordinary Differential Equations
  - forward Euler Method
  - Heun's method (RK2)
  - Ralston's third-order method (RK3)
  - Runga-Kutta method of order 4 (RK4)
- Root Finding Algorithms
  - Bisection Method
  - Newton's Method
  - Chord Method
- Constraint Optimization
  - Projected Gradient Descent

It should be noted that the analysis of numerical methods occurred at fixed operating conditions. It was assumed that the results would apply to the range of operating conditions that were then considered during optimization. This is a reasonable assumption, as the range of operating conditions in optimization was limited and included the fixed operating conditions, and thus no new numerical instability or performance change should be introduced.

In this section, we will introduce these methods and provide a brief overview of their key features. Additionally, we will thoroughly evaluate their strengths and weaknesses, and explain our rationale for selecting each method for our analysis

3.1 Ordinary Differential Equations

The eight differential equations given by Equation 4 and Equation 5, describing the mass and energy across the unit, take the form of an initial value problem (IVP) (i.e Equation 24). Specifically, the differential equations are bounded by the length of the reactor ($z \in [0, 7]$), and the initial conditions of Equation 4 and Equation 5 are given by the feed inlet conditions and the inlet temperature of the reactor. The initial conditions used in the modelling can be seen in Table 5.

$$\begin{cases} y'(t) = f(t, y(t)) \text{ for } t > 0 \\ y(0) = y_0 \end{cases} \tag{24}$$

Initial Condition of	Symbol	Value	Unit
CO	$F_{1,0}$	10727.9	kg/hr
CO_2	$F_{2,0}$	23684.2	kg/hr
CH_3OH	$F_{3,0}$	756.7	kg/hr
H_2	$F_{4,0}$	9586.5	kg/hr
H_2O	$F_{5,0}$	108.8	kg/hr
CH_4	$F_{6,0}$	4333.1	kg/hr
N_2	$F_{7,0}$	8071.9	kg/hr
Temperature	T_0	523.0	K

Table 5: Initial conditions of the eight differential equations describing the rate of composition of the seven species and temperature along the reactor

To obtain approximations to the initial value problems on the bounded time interval [0,7], we adopted the finite difference approach. Our discrete approximation will consist of $N+1$ real numbers $\{u_n\}_{n=1}^{N}$, where each u_n is an approximation of the value $y(t)$ at the mesh point $t = t_n$. We have decided to implement an evenly spaced mesh grid, with a constant mesh size h.

With this specified configuration, we are able to implement a series of ordinary differential equations (ODE) solvers, including the forward Euler, Heun's, third-order Runge-Kutta (RK3), and fourth-order Runge-Kutta (RK4) method. These methods are known for their stability and accuracy in solving ODEs, and we will compare their properties to determine which is most appropriate for our model.

In general, the forward Euler method is the simplest and most straightforward of the four methods, but it may not always be the most efficient or accurate. On the other hand, Heun's, RK3 and RK4 methods offer higher accuracy and more stability, but at a higher computational cost. We have considered these factors in our analysis.

In the following sections, we will explain the underlying theory and practical applications of each method, and evaluate their stability and accuracy to support our arguments.

3.1.1 Forward Euler Method

We first introduce the forward Euler Method. By approximating $y'(t)$ at $t = t_n$ with the difference quotient Equation 25 and replacing $f(t, y(t))$ with $f(t_n, u_n)$ we can represent the method in Equation 26 [16].

$$y'(t) \approx \frac{y(t_n + h) - y(t_n)}{h} \ , \ h > 0 \tag{25}$$

$$\begin{cases} u_0 = y_0 \\ u_{n+1} = u_n + hf(t_n, u_n), \ n = 0, 1, .., N-1 \end{cases} \tag{26}$$

The forward Euler method, benefits from its explicit nature and inexpensive implementation. However, the forward Euler method is only first order accurate meaning the truncation error tends to zero with order one, and has delicate stability properties. Namely, the method is not A-stable in reference to the problem in Equation 27. For methods that are not A-stable, we have conditional stability meaning that the asymptotic behaviour for large times is dependent of h relative to λ. For large values of λ, we would have to restrict the size of h and hence significantly increase the computational cost, to recover stability [16].

$$\begin{cases} y'(t) = \lambda y(t) \ , \ t > 0 \\ y(0) = 1 \end{cases} \tag{27}$$

3.1.2 Higher Order Runga-Kutta Methods

If we want to ensure increased stability and accuracy for a larger step size for h, then Heun's, RK3 and RK4 are expected to preform better than forward Euler. The higher order Runge-Kutta methods are generally more accurate and stable than the forward Euler method. The reason for this is that these methods use information about the derivative at multiple points, whereas the forward Euler method only uses information about the derivative at a single point. This allows the higher order Runge-Kutta methods to better approximate the true behavior of the system being modeled, which can lead to more accurate results.

Second Order Runga-Kutta Method: By replacing the unknown u_{n+1} by the result of a forward Euler step in the Crank-Nicolson method, we obtain the **Heun's method**, also known as the **improved Euler method** Equation 28. Heun's method is consistent (truncation error tends to zero) of order 2 [16].

$$u_{n+1} - u_n = \frac{h}{2}(f(t_n, u_n) + f(t_{n+1}, u_n + hf(t_n, u_n)) \tag{28}$$

Third Order Runga-Kutta Method: By increasing the number of interior stages of the method, we construct the third order Runga-Kutta method simply known as **RK3**. Refer to the subsection 6.1 for the detailed derivation of RK3. The recurrence equation of Runga-Kutta with three slope evaluations at each step takes the general form:

$$u_{n+1} = u_n + h(a_1K_1 + a_2K_2 + a_3K_3) \tag{29}$$

Where:

$$K_1 = f(t_n, u_n) \tag{30}$$
$$K_2 = f(t_n, +p_1hu_n + q_{11}hK_1)) \tag{31}$$
$$K_3 = f(t_n + p_2h, u_n + q_{21}hK_1 + q_{22}K_2) \tag{32}$$

A series of Taylor expansions around (t_n, u_n) results in the classical explicit Runge-Kutta method of order 3, abbreviated to **RK3**. The scheme is given by Equation 33 [16],

$$u_{n+1} = u_n + \frac{h}{9}(2K_1 + 3K_2 + 4K_3) \tag{33}$$

Where:

$$K_1 = f(t_n, u_n) \tag{34}$$
$$K_2 = f(t_n + \frac{h}{2}, u_n + \frac{h}{2}K_1) \tag{35}$$
$$K_3 = f(t_n + \frac{3h}{4}, u_n + \frac{3h}{4}K_2) \tag{36}$$

Fourth Order Runga-Kutta Method: The explicit Runge-Kutta method of order 4, known as **RK4** can be derived in a similar manner. The scheme is given by Equation 37 [16].

$$u_{n+1} = u_n + \frac{h}{6}(K_1 + 2K_2 + 2K_3 + K_4) \tag{37}$$

Where:

$$K_1 = f(t_n, u_n) \tag{38}$$

$$K_2 = f(t_n + \frac{h}{2}, u_n + \frac{h}{2}K_1) \tag{39}$$

$$K_3 = f(t_n + \frac{h}{2}, u_n + \frac{h}{2}K_2) \tag{40}$$

$$K_4 = f(t_n + h, u_n + hK_3) \tag{41}$$

RK3 and RK4 are consistent of order three and four respectively. Meaning that the truncation error converges to zero as $h \to 0$ with order three and four respectively. The RK3 and RK4 was derived with the assumption that the chosen step size (i.e h) was 'sufficiently small'. In subsubsection 4.2.1, we will investigate which step size is suitable for this, solving the differential equations in context of this modelling process.

3.2 Root Finding Algorithms

Root finding is a crucial step in modeling the separator, as it allows us to determine the vapor flow rate F_v calculated from the root of the Rachford-Rice equation 11. However, finding the roots of this equation is a non-trivial task since there is no closed form solution. In such cases, we must use numerical methods, such as the bisection, Newton's, and chord method, to approximate the roots of the function.

The Rachford-Rice equation has only one root within the bounds of $[0.60, 0.95]$, and we know that $f(0.60)f(0.95) \leq 0$ for this function. The bounds are the reasonable expectation of the value for the range of operating conditions that were considered in optimization. These conditions provide us with sufficient criteria to implement the bisection method, which is guaranteed to converge to an approximate solution of the root within the specified bounds. An addition advantage of the bisection method is that it avoids costly calculations of the derivative. However, the bisection method has relatively slow convergence, especially for our desired highly accurate approximation with an error tolerance of $\epsilon = 10^{-10}$. For this reason, we suggest that it is necessary to use iterative root-finding methods that have faster convergence rates, such as the chord and Newton's method, to obtain the desired accuracy within a reasonable amount of time. Provided that the solution lies within the bounds of $[0.60, 0.95]$ an initial guess of 0.76 was used for both Newton's and the chords method.

In the remainder of this section, we will explain the underlying theory and practical applications of each method, and evaluate their convergence speed relative to desired accuracy to support our arguments.

3.2.1 Bisection Method

We first introduce the bisection method. The bisection method is a bracketing method that is used to find the root of a given function, $f(x)$, within a specific interval $[a, b]$. It is based on a consequence of the intermediate value theorem 1 [16]. It capitalizes on this theorem by iteratively dividing the interval $[a, b]$ and choosing the sub-interval on which $f(x)$ changes sign.

Thereom 1 *Let $f : [a, b] \to R$ be continuous on the interval [a,b] and assume $f(a)f(b) \leq 0$. Then there exists $\alpha \in [a, b]$ such that $f(\alpha) = 0$*

Since the length of interval at each iteration is halved, it is possible to derive a prior error bound and hence quantify the rate of convergence. Given that the function f satisfies Theorem 1 it holds that for a root $\alpha \in [a, b]$:

$$|x_k - \alpha| \leq \frac{b - a}{2^k} \tag{42}$$

As mentioned above, to ensure convergence a and b was set to equal 0.60 and 0.95 respectively. These values are our expectation for what F_V/F should be for the explored range of operating temperature and pressures. In addition, we set an error tolerance of $\epsilon = 10^{-10}$. This level of tolerance was chosen as a trade-off between accuracy and number of iterations required of the explored methods. Using Equation 42, we can derive a lower bound of 32 iterations for the bisection method to converge to a root of Equation 11.

$$\frac{b-a}{2^k} \leq \epsilon \implies \frac{0.95-0.6}{2^k} \leq 10^{-10} \implies k \geq \frac{\log(0.35)}{\log(2)} \implies k \geq 31.745 \tag{43}$$

3.2.2 Newtons Method

Secondly, we will introduce Newton's method (i.e Equation 44), also known as Newton-Raphson method. Newton's method is an iterative method based on approximating the function with a linear line tangent to the curve at a given point, and then using the x-intercept of the tangent line to find the next approximation to the root.

$$x_{k+1} = x_k - \frac{f(x_k)}{f'(x_k)}, \ ,k = 0, 1, ... \tag{44}$$

The number of iterations required for Newton's method depends on several important factors, including the initial guess for the root and the accuracy of the derivative calculations. The derivative of Equation 11 was computed analytically [13]. Unlike the bisection method, it is not possible to derive a lower bound for the number of iterations needed for Newton's method. However, we know that the convergence rate of Newton's method can be quadratic, super-linear, or linear, depending on the smoothness of the f and the proximity of the initial guess to the true root.

Newton's method is expected to converge faster than the bisection method, as long as f is sufficiently smooth and the initial guess is close to the root. This is because Newton's method has quadratic convergence, which can only be violated if $f'(\alpha) = 0$ at the root α. However, this is not the case for our function, so we can expect quadratic convergence.

3.2.3 Chord Method

Lastly, we introduce the Chord Method (i.e Equation 45) which is similar to Newton's Method but approximates $f'(x)$ with some fixed number $q \in R$. Namely, we will take this fixed number to be the the derivative at the initial guess x_0.

$$x_{k+1} = x_k - \frac{f(x_k)}{f'(x_0)}, k = 0, 1, ... \tag{45}$$

Like Newton's method, we can not derive a lower bound of iterations. However, based on the convergence of fixed point methods (please refer to [16] for more in-depth analysis of fixed point methods), the chord method is guaranteed to converge linearly for an initial guess sufficiently close to the root α provided that:

$$|1 - \frac{f'(\alpha)}{f'(x_0)}| < 1 \tag{46}$$

In general the convergence is only linear, thus we expect slower convergence than Newton's method.

3.3 Optimization with Inequality Constraints

To perform the final optimization, we are required to solve an optimization problem with inequality constraints. The objective function we will use is the maximization of the methanol flowrate exiting the separator. The syngas feed flowrate of the process is fixed, thus by maximizing this objective, it it equivalent to maximizing the carbon efficiency of the process. The carbon efficiency of the process is the percentage of carbon dioxide converted into methanol. This objective function is representative of the overall economic and environmental status of the process, and has been used widely in literature [4, 9, 8]. Lastly, it is a simple objective function, thus not requiring detailed costing of the process.

The decision variables that were considered are the carbon ratio of the reed (the ratio of CO to $CO + CO_2$), reactor inlet temperature, separator temperature and separator pressure. These were chosen as the most important operating parameters whose value has a direct impact on the amount of methanol produced. The total carbon flowrate to the process was kept constant, but the ratio of CO to $CO+CO_2$ varied. The constant carbon

flowrate maintained a reactant basis that ensured that an increase methanol flowrate did not just result from having more reactants present. The composition of other flowrates in the syngas feed was not optimized. The feed to the process was assumed to be constant during optimization, its value taken from literature and the full composition shown in the appendices' Table 13.

The constraints arise from the physical and safety limitations of the system which impose bounds on the decision variables [14, 5]. A flask tank utilizes a pressure drop to separate components and thus needs to be operating at a lower pressure than its feed. Thus the maximum separator pressure was limited to being 5 bar less than the maximum reactor operating pressure. The carbon ratio bounds are between 0 and 1. The upper bound of the reactor inlet temperature was set to ensure no catalyst deactivation would occur (585 K) [10]. The lower bound was determined by ensuring the minimum approach temperature between the reactor, and the boiling water in its shell was not violated [14]. As the shell temperature was 490 K, the minimum reactor temperature possible was 500 K. Similarly, the minimum temperature achievable by the heat exchanger prior to the separator set the minimum separator temperature to be 308 K, as cooling water is used as the coolant. The separator operating pressure was taken from literature to be restricted to between 50 bar to 75 bar to ensure safe operating conditions [4].

A base case was used to compare the optimization results too, in order to analyze the improvements that are made. The operating conditions of the base case were taken from literature and full details can be found in Table 12 [4, 3]. The base case was additionally used as the initial guess for the value of the decision variables in optimization. Optimization was performed using projected-gradient descent, as this optimization routine accounts for inequality constraints in the problem.

3.3.1 Projected Gradient Descent

Projected gradient descent is an optimization algorithm which is used to the find the minimum value of an objective function with inequality constraints. It works by taking steps in the direction of the negative gradient of the objective function, and at each projecting the points into the feasible region that satisfies the constraints. The projection ensures that the optimal solution does not violate any constraints.

One advantage of projected gradient descent is that it is relatively simple to implement and can be applied to a wide range of optimization problems. It is also relatively efficient, as it only requires the computation of the gradient of the objective function, rather than the Hessian matrix, which is needed by some other optimization algorithms. Additionally, projected gradient descent can handle constraints that are non-differentiable, such as integer or binary constraints, which can be difficult for other methods to handle.

However, projected gradient descent also has some limitations. In particular, it can be sensitive to the choice of the step size, which can affect the convergence rate and the quality of the solution. It can also be slow to converge in high-dimensional problems, where the number of variables is large. Finally, projected gradient descent is a first-order method, which means that it only uses information about the gradient of the objective function, and not the Hessian matrix or higher-order derivatives. This can limit the accuracy of the solution in some cases.

4 Results

4.1 Overall Results

The objective of this report is to develop an accurate and efficiently computed model of the process in order to perform optimization. In this section, we first present our findings regarding the analysis of numerical methods used in the modeling. Next, we validate that our model describes the physical system. Lastly, we discuss the results from optimization of the process.

For one, there are couple notable findings in the numerical methods analysis. Firstly, RK3 and RK4 demonstrate larger stability regions than forward Euler and Heun's method. We observed that RK3 and RK4 share a similar stability regions. In addition, as expected Newtons method showed the fastest convergence compared to the bisection and chord method. We favoured RK4 and Newtons method in the modeling. This is because RK4 had the highest convergence order and allowed for a large step size and Newtons method converged in the least number of iterations.

The separator and reactor, solved using RK4 and Newton's method respectively, were validated, and it was shown that the relative error was less than 1% for all outputs of the units that were tested. Optimization was performed, leading to a 14.2% increase in the methanol production from the base case, for a fixed feed to the process.

4.2 Numerical Methods Comparison

4.2.1 Solving Differential Equations

In order to perform error analysis, a solution is required. Since we do not have a closed-form solution to Equation 4 and Equation 5, we first derived an approximation of our true solutions before conducting error analysis. To obtain an approximation to the true solution for all seven chemical component profiles and the temperature in the reactor, the forward Euler method was used with a step size of $h = 0.0001$. From Figure 2, we can see that there are no oscillations indicating that approximation is stable for $h = 0.0001$, and hence could act as a suitable substitution to the true solution.

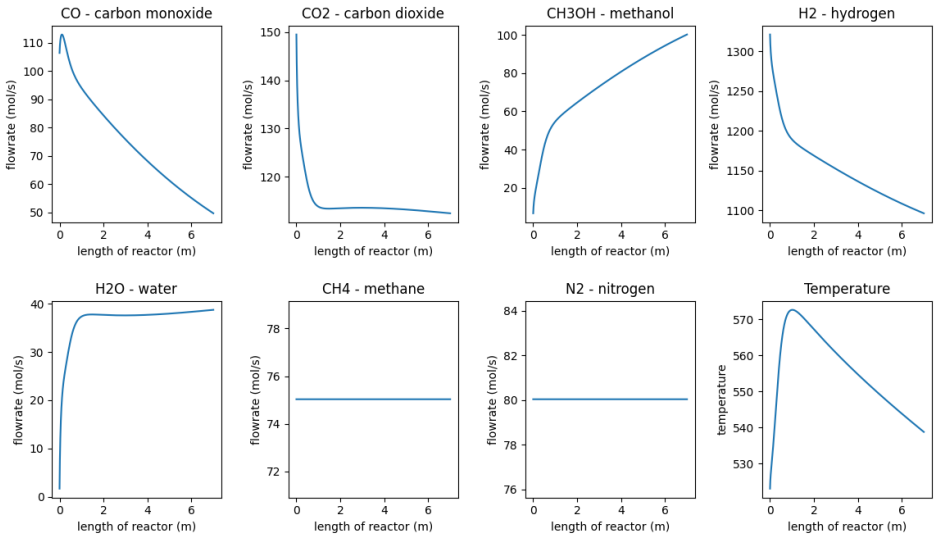

Figure 2: Stable approximation for all species and temperature in reactor using forward Euler with step size h= 0.0001

However, the forward Euler method has rather delicate stability properties. Specifically, the forward Euler method is not A-stable and hence its expected that as the step size increases the accuracy of the forward Euler approximation deteriorates rapidly due to the lack of absolute stability. To better understand this relationship, we compared the stability of forward Euler with other methods using a range of step sizes. We concentrate the analysis on the reactor profile of carbon monoxide (i.e CO). Figure 3, shows the approximations produced by the forward Euler, Heun's, RK3 and RK4 for step sizes $h = 0.02, 0.03, 0.04, 0.05, 0.06$. In accordance with the absolute stability theory, the forward Euler method requires the smallest step size too ensure the correct asymptotic behaviour of the solution. Namely, we see that for $h \leq 0.04$ the forward Euler method is stable, and starts to oscillate if the step size is increased further. Heun's method also produces unstable results for $h > 0.04$, however the solution produced by Heun's method at $h = 0.05$ is more accurate than that of the forward Euler method. The RK3 and RK4 graphs, share similar asymptotic behaviour for a given step size. We can observe that both method are more stable than the forward Euler and Heun's method for larger step sizes. Namely, RK3 and RK3 produces accurate results up to and including $h = 0.05$. Nevertheless, if the step size increased further (i.e $h > 0.05$) the solution produced by RK3 and RK4 also starts to diverge.

Now we redirect our analysis to include all species and the temperature in the reactor for a fixed step size $h = 0.05$. In Figure 4, we observe similar stability proprieties for all four methods as seen in Figure 3. The

forward Euler method experiences the greatest amount of oscillations, followed by the Heun's method. Clearly RK3 and RK4 produces the most stable solution, with no clear stability region difference between the two methods. There is no difference between the methods in approximating the profiles of CH_4 and N_2. This is because they are inert chemical species, that do not react therefore maintaining a constant flow rate throughout the reactor, with no rate of change.

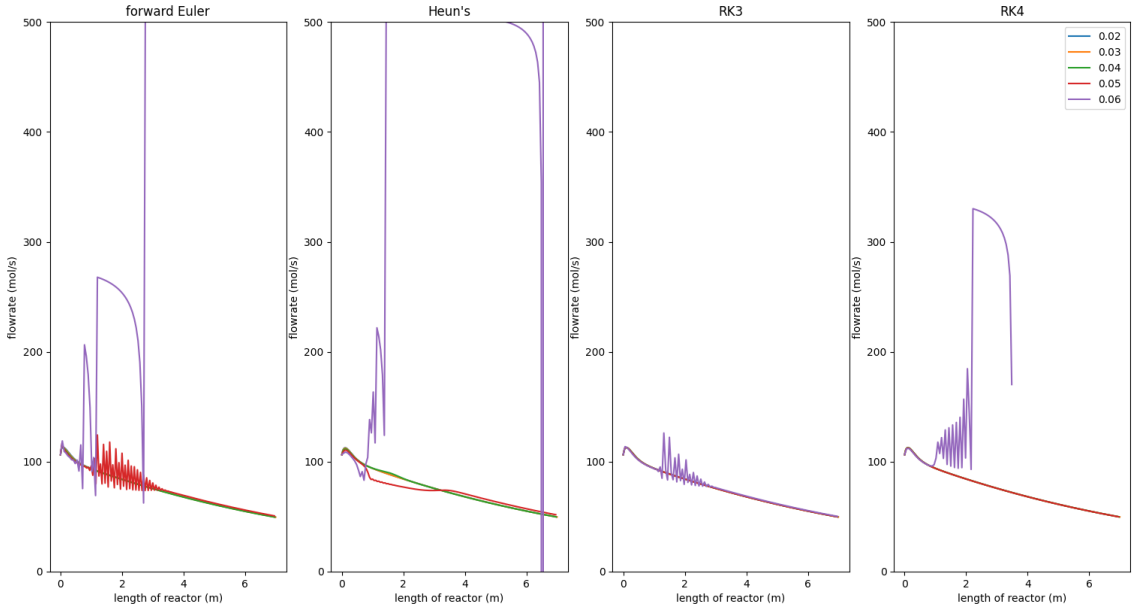

Figure 3: Approximate solution for CO in reactor simulation using forward Euler, Heun's, RK3 and RK4 with step sizes $h \in [0.02, 0.06]$

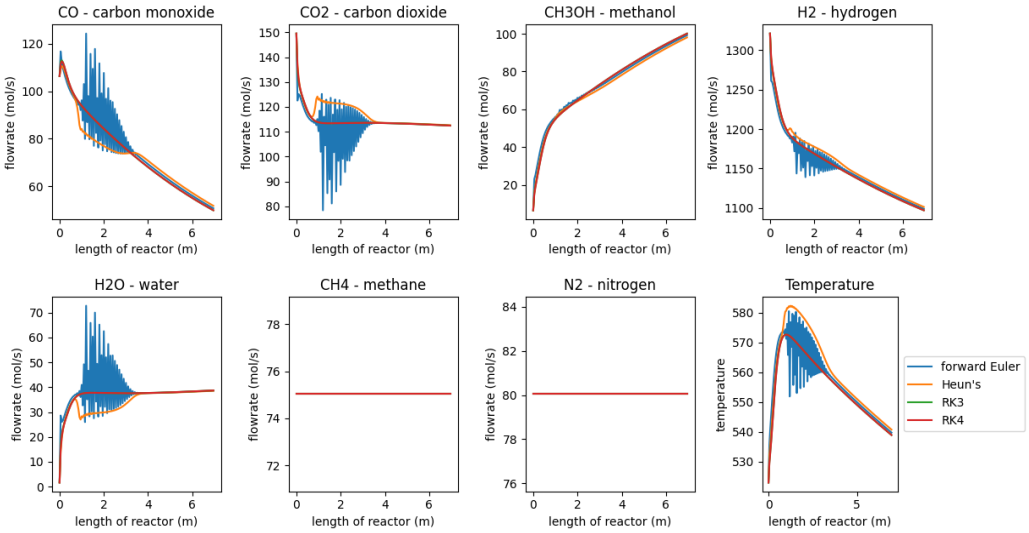

Figure 4: Approximate solution for all species and Temperature in reactor given step size $h = 0.05$

Finally we studied the convergence order of the four methods Figure 5. This was accomplished by obtaining the reactor profiles for step sizes $h \in [0.001, 0.03]$ (for which all four methods are stable) and computing the errors of the resulting approximation when compared to the true solution. The stable approximation, seen in Figure 3, was used as an approximation to the true solution, and the errors were computed using the infinity

norm. Again, the analysis was concentrated for carbon monoxide. As seen in Table 6 and in accordance with the theory, first order convergence is observed for the forward Euler method, second order convergence for Heun's method, third for RK3 and fourth for RK4.

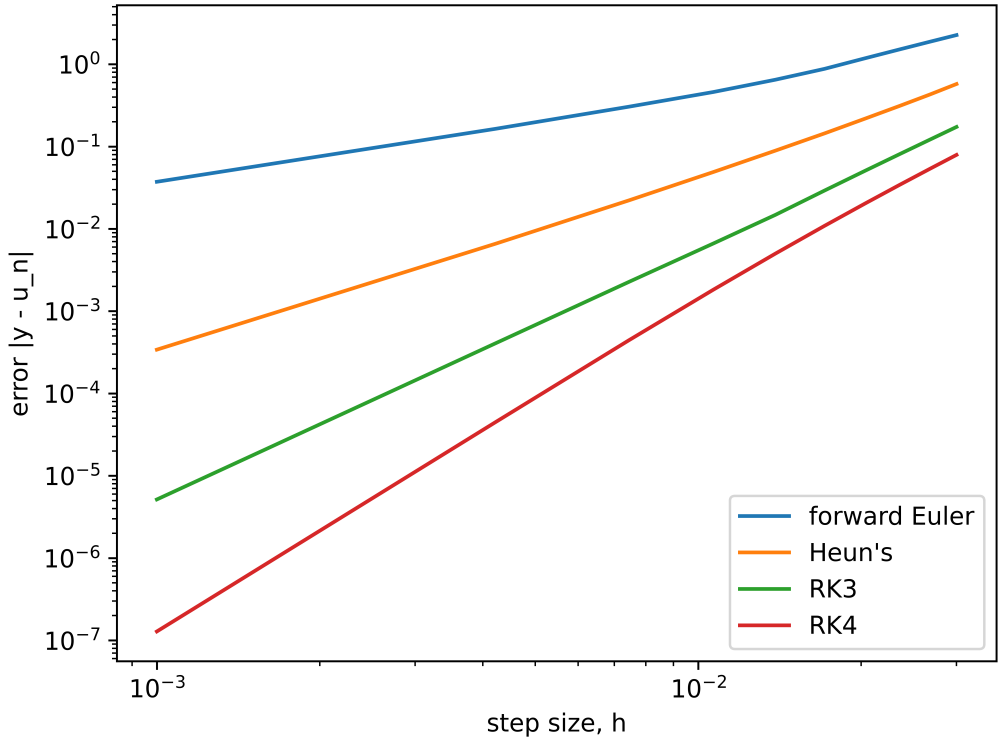

Figure 5: Errors on a log-log scale plotted against the step size (h) for the forward Euler method, Heun's, RK3 and RK4 method

Method	**Convergence order (i.e slope of error)**
forward Euler	1.21
Heun's	2.19
RK3	3.06
RK4	3.92

Table 6: Convergence order measured by the slope of the errors as a function of the step size (h) on a log-log scale

4.2.2 Root Finding

To obtain the vapor flow rate F_v, we solve for the root of the Rachford-Rice Equation 11. The results show the convergence towards a root using all our three iterative methods, bisection, chord and Newton's. Namely, we achieved convergence for the chord method since for the initial guess $x_0 = 0.76$ and root $\alpha = 0.88157$ we have that $|1 - \frac{f'(0.88157)}{f'(0.75)}| = 0.3147$ which is less than 1 as required by fixed point method convergence Equation 11. In addition as expected Newtons method converged in the least number of iterations. Specifically, Newton's method converged in 19 iterations, roughly 10 less iterations required for both the chord and bisection methods (seen in Table 7). Satisfying the lower bound on the number of iterations to guarantee the error tolerance of $\epsilon = 10^{-10}$ Equation 43, the bisection method converged in 32 iterations.

In Figure 6, we observe the linear convergence of the chord method. In addition we can see that the errors of Newton's method decreases much fast, reflecting the quadratic convergence property. Specifically, we can observe close to quadratic convergence in close proximity to the root for Newtons method (seen by the blue dotted line in Figure 6). Lastly, we can observe that the error of the bisection method oscillates indicating that it has non-monotonic convergence.

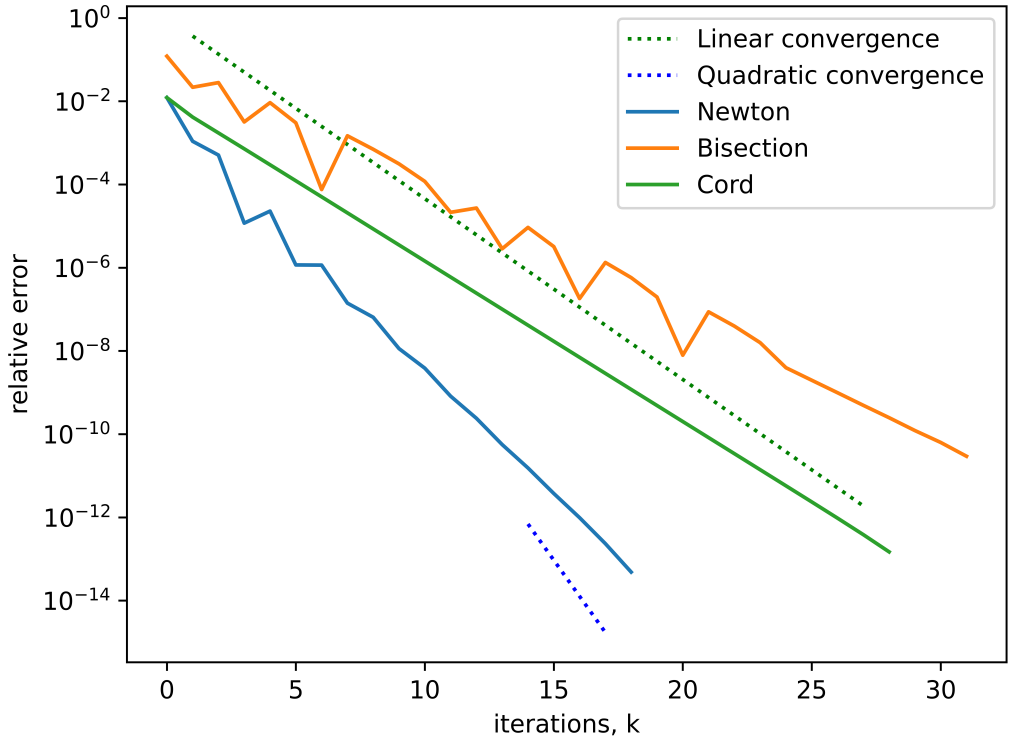

Figure 6: Log linear plot of the error as a function of the number of iterations for the bisection, chord and Newton's method

Method	**Number Iterations**	**Vapor flow rate F_v**
Bisection	32	0.881574027723
Chord	29	0.881574027738
Newton	19	0.881574027738

Table 7: Number of iterations and final solution for bisection, chord and Newton's method

4.3 Model Validation

Model validation was done to verify that the detailed modeling of the reactor and separator was an accurate representation of the physical system.

Reactor Model: For the reactor, we compared our simulation to industrial data for a methanol synthesis reactor [3]. The results were comparable, as we set the reactor operating conditions, feed specification, and other modeling assumptions to that specified by [3] (see Table 11 for values). As seen in Table 8 and 9, there is strong agreement between our predicted reactor outlet stream and what was obtained in industry. To model any complex system, simplifications and assumptions are required. Famously put, "all models are wrong, but some are useful". The source of the difference between the modeled and true data, is likely from simplification

	Feed specifications	Modeled outlet stream	Industry outlet stream	Relative error (%)
Temperature (K)	498	530	528	0.3788

Table 8: Comparison of modeled outlet stream conditions to industry data - Temperature

Component's flow rate (kg/h)	Feed specifications	Modeled outlet stream	Industry outlet stream	Relative error (%)
CO	10728	4955.4	4921.0	0.69904
CO_2	23684	18317	18316	0.00546
CH_3OH	756.70	11268	11283	0.13294
H_2	9586.5	8018.2	8013.7	0.05615
H_2O	108.80	2305.7	2309.3	0.15589
CH_4	4333.1	4333.1	4333.1	0.00000
N_2	8071.9	8071.9	8071.9	0.00000

Table 9: Comparison of modeled outlet stream conditions to industry data - Component's flowrates

assumptions that we made in reactor modeling, for example not accounting for intra-particle diffusion. Due to the fact that the relative error of the model is low, the mathematical model and code implementation has been validated to represent reality somewhat.

Separator Model: The accuracy of the separator's modeling depends almost entirely on the correct prediction of the vapor liquid equilibrium, which depends on the estimate of the equilibrium ratios (K) for each component. Accurate K-value prediction requires that not only is the separator iterative procedure working both in finding the correct K-values and vapor fraction (F_V/F), but that additionally the correct finding if the roots of the cubic equations in PR-EOS. Thus, to confirm the validity of the separator model and the implementation of PR-EOS, we compared the K-values for each component to K values obtained from COCO. COCO is a free-of-charge compliant steady-state chemical simulation environment [15]. We used a simulator for validation, rather than experimental data because since the system is a non-binary mixture of components, the K-values are unobtainable from literature. As seen in Figure 7, for a range of temperature values their is agreement between the equilibrium ratio, the K-value, predicted by our model and the value generated by the simulator. Thus, over a range of operating temperatures our separator model has been validated.

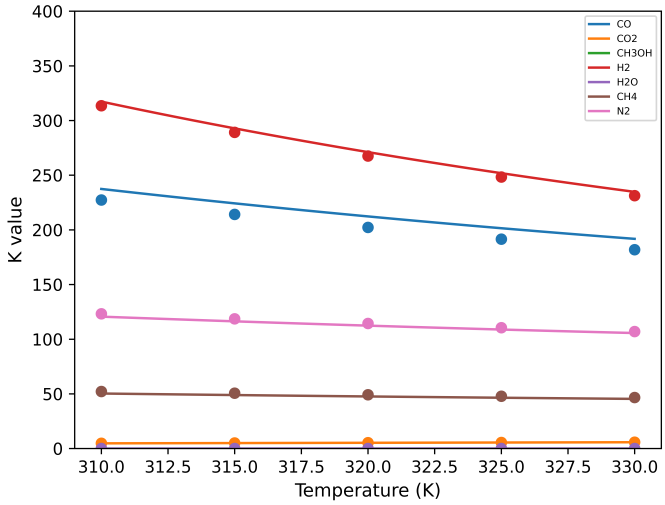

Figure 7: Comparison of K values obtained from model (line) to values obtained from COCO simulation (dots)

4.4 Constraint Optimization

Optimization was performed, and the final results of the decision variable and the maximum methanol flowrate achieved are shown in the Table 10. We were able to increase the methanol production from the base case value of 98.8 mol/s to 112.8 mol/s which is an improvement of 14.2%. Thus, optimization of the process was successful. The percentage improvement is relatively low, and the likely reason for this is that the process has existed for many years, and thus the base case taken from literature has previously been optimized [10]. The optimal value of some of the decision variables are on the boundary of the constraints, which is possible in optimization with inequality constraints. One can see from Figure 8, that the optimization routine was highly sensitive to the initial guess of the problem. From the same figure, we can also see that most of the change in the objective function's value occur at the beginning of the method, after which the progress diminishes. In future work, adaptive step size should be explored. This method may aid in finding a better optimal, as step sizes specific to the progress in the routine can be used to ensure faster convergence.

	Unit	**Base case**	**Optimized case**
Methanol flowrate	mol/s	98.8	112.8
Reactor inlet temperature	K	500	500
Separator inlet temperature	K	315	308
Separator pressure	bar	60	68.3
Carbon ratio		0.529	0.854

Table 10: Comparison of base case to optimization case

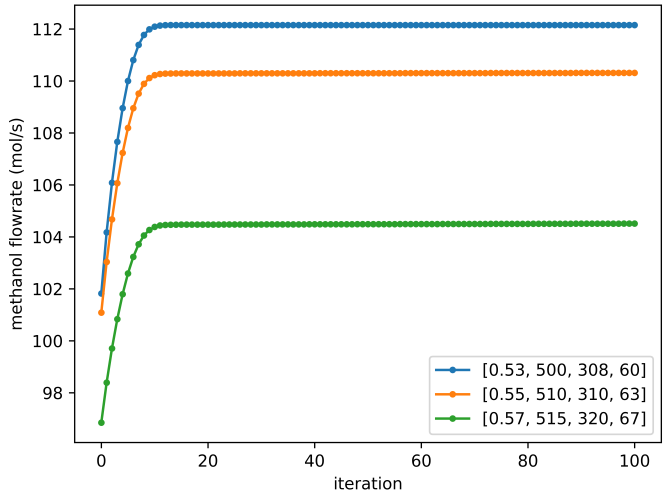

Figure 8: Project gradient descent iterations for different initial conditions [carbon ratio, reactor temperature, separator temperature and separator pressure] showing the sensitivity of the method to these guesses

It is noted that the values that were arrived at are highly sensitive to the syngas feed to system. Syngas is produced from a wide range of waste and biomass feedstocks, and as the composition of feedstock varies, so does the syngas produced. If a system had a different feed, the optimal operating conditions would be different. The code is set up and the optimization could be re-run for these alternative feeds.

5 Conclusion

In this study, we developed a numerical model to simulate the conversion of CO_2 into methanol, which involved solving a series of complex tasks. These tasks included approximating the solution of ordinary differential

equations that modeled the flow rates of various species in the process, finding roots of the Rachford-Rice equation to determine the vapor-liquid equilibrium, and optimizing production subject to constraints.

To solve the ordinary differential equations, we compared the stability of four different methods: the forward Euler method, Heun's method, RK3, and RK4. We found that all methods were stable for small step sizes within the range of $h \in [0.0001, 0.04]$, but only RK3 and RK4 were stable for larger step sizes within the range of $h \in [0.0001, 0.05]$. This suggests that RK3 and RK4 may be more suitable for solving the ordinary differential equations in this particular process.

To find the roots of the Rachford-Rice equation, we used three root-finding algorithms: the bisection method, Newton's method, and the chord method. Our results showed that all three methods were able to find the optimal solution, with Newton's method demonstrating the fastest convergence rate due to its close to quadratic convergence.

We performed optimization to maximize the methanol flow rate subject to constraints on the physical and safety limitations of the system. The optimization was successful, increasing the methanol production from 98.8 mol/s to 112.8 mol/s, or a 14.2% improvement. This demonstrates the effectiveness of our optimization approach in finding an optimal solution that increases the methanol production.

References

[1] S. Abrol and C. M. Hilton. Modeling, simulation and advanced control of methanol production from variable synthesis gas feed. *Computers & chemical engineering.*, 40:117–131, 2012.

[2] K. M. Bussche and G. Froment. A steady-state kinetic model for methanol synthesis and the water gas shift reaction on a commercial cu/zno/al2o3 catalyst. *Journal of Catalysis*, 161(0156), 1996.

[3] L. Chen, Q. Jiang, Z. Song, and D. Posarac. Optimization of methanol yield from a lurgi reactor. *Chemical Engineering & Technology*, 34:817–822, 2011.

[4] R. O. dos Santos, L. de Sousa Santos, and D. M. Prata. Simulation and optimization of a methanol synthesis process from different biogas sources. *Journal of Cleaner Production*, 186:821–830, 2018.

[5] S. Fogler. *Elements of Chemical Reaction Engineering.* Prentice Hall, 2004.

[6] A. Goeppert, M. Czaun, J.-P. Jones, G. Prakash, and G. Olah. Cheminform abstract: Recycling of carbon dioxide to methanol and derived products - closing the loop. *Chemical Society reviews*, 46, 06 2014.

[7] D. Green and R. Perry. *Perry's Chemical Engineers' Handbook.* McGraw-Hill Companies, eighth edition, 2008.

[8] H. Kordabadi and A. Jahanmiri. Optimization of methanol synthesis reactor using genetic algorithms. *Chemical Engineering Journal*, 108(3):249–255, 2005.

[9] H.-W. Lim, H. J. Jun, M.-J. Park, and H.-S. Kim. Optimization of methanol synthesis reaction on cu/zno/al2o3/zro2 catalyst using genetic algorithm: Maximization of the synergetic effect by the optimal co2 fraction. *Korean Journal of Chemical Engineering*, 27, 2010.

[10] W. L. Luyben. Design and control of a methanol reactor/column process. *Industrial & Engineering Chemistry Research*, 49(13):6150–6163, 2010.

[11] F. Manenti, S. Cieri, and M. Restelli. Considerations on the steady-state modeling of methanol synthesis fixed-bed reactor. *Chemical engineering science*, 66(2):152–162, 2011.

[12] B. Poling, J. Prausnitz, and J. O'Connell. *The Properties of Gases and Liquids.* McGraw-Hill Companies, 2001.

[13] S. Skogestad. Chemical and energy process engineering, 2009.

[14] R. Turton, J. Shaeiwitz, D. Bhattacharyya, and W. Whiting. *Analysis, Synthesis, and Design of Chemical Processes.* Prentice Hall, 2003.

[15] J. van Baten, R. Baur, H. Kooijman, R. Taylor, and W. Barret. Cape open to cape open simulation environment, 2022.

[16] S. Xu. *An Introduction To Scientific Computing with MATLAB and Python Tutorials.* CRC Press, 2022.

6 Appendix

6.1 Runga-Kutta Order 3 Derivation

The recurrence equation of Runga-Kutta with three slope evaluation at each step takes the general form of Equation 47. For simplicity we proceed with the notation, $f_n = (t_n, u_n)$, $f_t = \frac{\partial f(t_n,u_n)}{\partial t}$, $f_y = \frac{\partial f(t_n,u_n)}{\partial y}$.

$$u_{n+1} = u_n + h(a_1K_1 + a_2K_2 + a_3K_3) \tag{47}$$

Where: $K_1 = f(t_n, u_n)$, $K_2 = f(t_n, +p_1hu_n + q_{11}hK_1)$, $K_3 = f(t_n + p_2h, u_n + q_{21}hK_1 + q_{22}K_2)$

The Taylor expansion of $u_{n+1} = y(t_n + h)$ around t_n up to $O(h^4)$ is given by Equation 48.

$$u_{n+1} = u_n + hf + \frac{h^2}{2}(f_t + f_yf) + \frac{h^3}{2}(f_{tt} + 2f_{ty}f + f_tf_y + f_{yy}f^2 + f_y^2f) + O(h^4) \tag{48}$$

Expression Equation 48 was simplified by using the following properties:

$$y'_n = f(t_n, u_n)$$

$$y''_n = \frac{d}{dt}f(t_n, u_n(t_n)) = f_t + y'f_y = f_t + ff_y$$

$$y'''_n = \frac{d}{dt}(f_t + ff_y) = f_{tt} + 2f_{ty}f + f_tf_y + f_{yy}f^2 + f_y^2f$$

Now we proceed by Taylor expanding K_2 and K_3 around (t_n, u_n) which gives us the Equation 49 and Equation 50 respectively. Both expressions Equation 49 and Equation 50 have been simplified by using $K_1 = f$.

$$K_2 = f + p_1hf_t + q_{11}hff_y + \frac{1}{2}(p_1^2h^2f_{tt} + 2p_1q_{11}h^2ff_{ty} + q_{11}^2h^2f^2f_{yy}) + O(h^3) \tag{49}$$

$$K_3 = f + p_2hf_t + h(q_{21}f + q_{22}k_2)f_y + \frac{1}{2}((p_2^2h^2f_{tt} + 2p_2h^2(q_{21}f + q_{22}k_2)f_{ty} + h^2(q_{21}f + q_{22}k_2)^2f_{yy}) + O(h^3) \tag{50}$$

Substituting K_1 along with expression Equation 49 and Equation 50 in Equation 47 and grouping terms matching expression Equation 48, gives Equation 51

$$\begin{aligned} u_{n+1} = u_n \\ + h(a_1 + a_2 + a_3)f \\ + h^2(a_2(p_1f_t + q_{11}ff_y) + a_3(p_2f_t + q_{21}ff_y + q_{22}ff_y)) \\ + h^3\frac{a_2}{2}({p_1}^2f_{tt} + 2p_1q_{11}ff_{ty} + q_{11}^2f^2f_{yy}) \\ + a_3(q_{22}(p_1f_tf_y + q_{11}f_y^2f) + \frac{1}{2}(f_{tt}p_2^2 + f_{yy}(q_{21} + q_{22})^2f^2 + 2f_{ty}p_2f(q_{21} + q_{22}))) + O(h^4) \end{aligned} \tag{51}$$

Matching terms in expression Equation 48 and Equation 51 yields the following equations:

1. $a_1 + a_2 + a_3 = 1$
2. $a_2p_1 + a_3p_2 = \frac{1}{2}$
3. $a_2q_{11} + a_3(q_{21} + q_{22}) = \frac{1}{2}$

4. $a_2 p_1^2 + a_3 p_2^2 = \frac{1}{3}$
5. $a_2 q_{11} + a_3(q_{21} + q_{22}) = \frac{1}{2}$
6. $a_2 p_1 q_{11} + a_3 p_2(q_{21} + q_{22}) = \frac{1}{3}$
7. $a_3 q_{22} p_1 = \frac{1}{6}$
8. $a_2 q_{11}^2 + a_3(q_{21} + q_{22})^2 = \frac{1}{3}$
9. $a_3 q_{22} q_{11} = \frac{1}{6}$

Setting equation equation (7) equal to (9) we obtain $q_{11} = p_1$. Subtracting equation (8) from (6) we obtain $p_2 = q_{21} + q_{22}$. Plugging in these results in the above equations we get that (2) and (3) are the same as well as (4) and (6).

Hence we are left with four nonlinear equations item 6.1 and and six unknowns $(a_1, a_2, a_3, p_1, q_{21}, q_{22})$.

1. $a_1 + a_2 + a_3 = 1$
2. $a_2 p_1 + a_3 p_2 = \frac{1}{2}$
3. $a_2 p_1^2 + a_3 p_2^2 = \frac{1}{3}$
4. $a_3 q_{22} p_1 = \frac{1}{6}$

The unknown coefficients can be solved by setting (an initial guess):

$$q_{11} = \frac{1}{2} \text{ and } p_2 = \frac{3}{4}$$

Given q_{11}, p_2 and solving the above four nonlinear equations we obtain the following coefficients

$$p_1 = \frac{1}{2}, p_2 = \frac{3}{4}, q_{11} = \frac{1}{2}, q_{21} = 0, q_{22} = \frac{3}{4}, a_1 = \frac{2}{9}, a_3 = \frac{3}{9}, a_4 = \frac{4}{9}$$

Which results in the classical explicit Runge-Kutta method of order 3, abbreviated to **RK3**:

$$u_{n+1} = u_n + \frac{h}{9}(2K_1 + 3K_2 + 4K_3)$$

where:

$K_1 = f(t_n, u_n)$

$K_2 = f(t_n + \frac{h}{2}, u_n + \frac{h}{2}K_1)$

$K_3 = f(t_n + \frac{3h}{4}, u_n + \frac{3h}{4}K_2)$

6.2 Reactor Constants Used During Model Validation

In order to allow for a fair comparison, the reactor constant's need to be set to the parameters of the industrial system [3]. These values are shown in Table 11.

6.3 Optimization Conditions

The Table 12 summarizes the base case operating conditions that were used as an initial guess for optimization, and as a basis to compare the final results too.

The following Table 13 details the composition of the syngas feed to the process that was kept constant except for the flowrates of CO and CO_2. The feed was based off industrial data found in literature for a typical feed composition [3]. The total carbon flowrate to the process was kept constant, but the ratio of CO and CO_2 was varied.

Parameter	**Symbol**	**Value**	**Units**
Void fraction of catalyst	ϵ_{cat}	0.285	
Density of catalyst	ρ_{cat}	1 190	kg/m^3
Activity of catalyst	a	1	
Internal diameter of reactor tube	D_{int}	0.04	m
Overall heat transfer coefficient	U	118.44	W/m^{2}K
Temperature of boiling water shell side	T_{shell}	485	K
Reactor length	z	7	m
Number of tubes	N_t	1620	
Number of species	N	7	
Number of reactions	n	3	

Table 11: Value of constants used in reactor mass and energy balance

	Unit	**Base case**
Methanol flowrate	mol/s	98.8
Reactor inlet temperature	K	500
Separator inlet temperature	K	315
Separator pressure	bar	60
Carbon ratio		0.529

Table 12: Base case values of the decision variables and methanol production rate

	Component flowrate in fixed syngas feed	**Unit**
CO and CO_2	255.8	mol/s
CH_3OH	6.560	mol/s
H_2	1321	mol/s
H_2O	1.678	mol/s
CH_4	75.03	mol/s
N_2	80.04	mol/s

Table 13: Syngas feed composition